Diurnal and subdiurnal effects of the atmosphere on the Earth rotation and geocenter motion

Olivier de Viron and Gaëtan Schwarzbaum
Royal Observatory of Belgium, Brussels, Belgium

Francois Lott
Laboratoire de Météorologie Dynamique, Ecole Normale Supérieure, Paris, France

Véronique Dehant
Royal Observatory of Belgium, Brussels, Belgium

Received 4 April 2005; revised 11 July 2005; accepted 5 August 2005; published 8 November 2005.

[1] The diurnal cycle in the atmospheric angular momentum (AAM) and in the wind and surface pressure fields is studied with a realistic atmospheric general circulation model (GCM) in which the AAM budget is very well closed. For this, we used a 1 year simulation. From a geodetic point of view, we find that this model predicts AAM variations at diurnal timescale which produce a polar motion near 0.2 milliarc second. Additionally, at the same period, the model predicts a geocenter motion of the order of a millimeter. These results are compared with those obtained with the National Centers for Environmental Prediction/National Center for Atmospheric Research and the European Centre for Medium-Range Weather Forecasts operational analysis data sets. As the AAM budget is not exactly closed in those two data sets, large quantitative differences with the GCM are found. These results witness that there are problems in using AAM values from the major weather prediction center to estimate the AAM and torques variation at diurnal and subdiurnal timescales. We have also computed, for the three models, the spherical harmonics decomposition of the diurnal and semidiurnal surface pressure signals. The results show large differences from one model to another, which advices carefulness when correcting gravity missions (as Gravity Recovery and Climate Experiment (GRACE), for instance) from the high-frequency effect of the atmosphere on the orbit, using operational analysis.

Citation: de Viron, O., G. Schwarzbaum, F. Lott, and V. Dehant (2005), Diurnal and subdiurnal effects of the atmosphere on the Earth rotation and geocenter motion, *J. Geophys. Res.*, *110*, B11404, doi:10.1029/2005JB003761.

1. Introduction

[2] The interaction between the Earth and its superficial layers (atmosphere, ocean and hydrology) is a major cause of changes in the Earth rotation for periods ranging between several hours and several years. In particular, and if we exclude the well-predicted oceanic tides, the atmosphere is known to dominate the Earth rotation variations between several hours and several years [see, e.g., *Barnes et al.*, 1983].

[3] The Earth rotation fluctuations can be decomposed into three different components: the variations of the rotation speed, associated with changes in the length of day (LOD), the motion of the solid Earth around its rotation axis, known as the polar motion, and the motion of the Earth rotation axis in space, known as precession-nutation. The effect of the atmosphere on Earth rotation can be studied by two different and complementary methods: (1) the angular momentum approach, in which the Earth-Atmosphere system is considered as isolated, in the sense that the variation of the angular momentum of the system are neglected, and the Earth rotation variations are computed from the change in the atmospheric angular momentum (AAM) and (2) the torque approach, for which the interaction between the solid Earth and the atmosphere is evaluated directly (see *Wahr* [1982] for more details about the two approaches). The two approaches are linked by the angular momentum budget equation of the atmosphere: the rate of change of the AAM is equal to the total torque acting on the atmosphere at the Earth/ocean surface.

[4] Each of the three components of the AAM is composed of two parts: a mass term (or pressure term) associated with a rigid rotation of the atmosphere with the Earth and a wind term (or motion term) associated with the relative motion of the atmosphere with respect to the Earth. The total torque is composed of an ellipsoid contribution (resulting from the pressure force and gravitational interac-

0148-0227/05/2005JB003761$09.00

tion between the Earth bulge and the atmosphere), a mountain torque related to the pressure acting on the topography, and a friction torque [see *Wahr*, 1982]. In general circulation models (GCMs), this latter torque is computed from the surface stress predicted by the model boundary layer turbulence parameterization. Additionally, the mountain torque is complemented by a torque related to surface stress due to the subgrid-scale orography parameterization (see *Lott and Miller* [1997] for the European Centre for Medium-Range Weather Forecasts (ECMWF) model and for the Laboratoire de Météorologie Dynamique (LMD) GCM).

[5] In this paper, we focus on the AAM changes in the diurnal band, which are very important for the nutation of the Earth. Indeed, the conservation of the Earth-Atmosphere angular momentum impose that the atmospheric motion at quasi-diurnal retrograde period is compensated by nutational motion of the solid Earth. This effect has been evaluated using the angular momentum approach, for instance by *Bizouard et al.* [1998], and using the torque approach by *Dehant et al.* [1996]. This last study has shown that the atmospheric effect on nutation, when evaluated using the torque approach, was too large by at least one order of magnitude with respect to the observed nutation of the Earth. This problem has been studied by *de Viron et al.* [2001] and *Marcus et al.* [2004]. They used data from the National Center for Environmental Research/National Center for Atmospheric Research (NCEP/NCAR) reanalysis model [*Kalnay et al.*, 1996] and show that the problem was in the torque approach, and comes from an ill-conditioned equation: the angular momentum budget has to be considered in an inertial frame, and in this frame the AAM variations are slow (diurnal retrograde in the rotating frame becomes low frequency in the inertial frame), which implies a small torque. As this small torque should result from a nearly exact cancellation between a large ellipsoidal torque (global effect of the atmospheric mass acting on the Earth bulge) and the local torques due to mountains and boundary layer stresses, it can only be obtained if the torques can be estimated with a very good precision, which could not be achieved with the NCEP/NCAR reanalysis data [*de Viron et al.*, 2001; *Marcus et al.*, 2004]. The quality of the S_1 wave in the NCEP reanalysis and ECMWF analysis has been discussed by *Ray and Egbert* [2004].

[6] In this paper, we used a 1 year simulation with the LMD atmospheric GCM [see, e.g., *Lott*, 1999]. The evolution of this GCM is never interrupted by any assimilation procedure (unlike the ECMWF and the NCEP models), which ensures a very good closure of the angular momentum budget. In this model, we analyzed the three components of the AAM budget, and deduce the predicted torques at diurnal and subdiurnal periodicities. In addition, we evaluate the effect on the Earth rotation and geocenter motion. We also compare the atmospheric forcing, for the frequencies allowed by each model sampling, to those computed from the output of the NCEP reanalysis and from the ECMWF reanalysis.

[7] The plan of the paper is as follows. Section 2 presents the different data sets used. Section 3 compares the diurnal cycles in flow field from the three data sets, focusing on those which matter for AAM and torques, that is the surface pressure and the barotropic wind (i.e., the wind integrated vertically over the pressure column). After this evaluation of the model performance, section 4 analyzes the AAM budget and some consequences on the Earth rotation parameters. Section 5 concludes and discusses the significance of the results from section 3 to the dealiasing of gravity missions, such as Gravity Recovery and Climate Experiment (GRACE) and Challenging Minisatellite Payload for Geophysical Research and Application (CHAMP) from the diurnal tides in the surface pressure. It also discusses the significance of the results in section 4 to the prediction of the diurnal variations of the EOP from the major prediction center operational analyses.

2. Simulation and Model Used

[8] The LMD GCM that we use is a grid point model, with a $2.5^\circ \times 2.5^\circ$ horizontal resolution and 19 vertical levels, most of them spanning the entire troposphere but a few of them are in the stratosphere. It is forced by climatological sea surface temperature and sea ice cover, a configuration for which its climatology is realistic [*Lott*, 1999]. In time, this model solves all adiabatic processes (advection plus pressure forces) explicitly, yielding a short temporal resolution ($dt = 30$ s). In this context, the adiabatic processes (radiation, boundary layer and subgrid-scale orography parameterizations) are called every 15 min only.

[9] Consistently, the solar forcing also varies along a climatologic annual cycle and includes a daily cycle. Most of the atmospheric minor species are fixed, except (1) the Ozone which varies as a function of time altitude and altitude using smooth analytical functions and (2) the water vapor which is an explicit predicted quantity of the model. Note that these species are essential for the upper level forcing of the tides, because they absorb short waves radiation. In this context it is noteworthy that our model only has four levels in the stratosphere (above 20 km). We found that it results in an underestimate of the contribution of Ozone to the forcing of the semidiurnal tide (O3 only explains 1/2 of the 1/2-diurnal tide in the model, while in reality, this number is rather 2/3; this was established through experiments where the SW diurnal cycle was not included in the SW radiation routines that call the 03).

[10] In this paper, we use a 1 year simulation of the LMD-GCM, and evaluate every hour the barotropic wind and the various surface stresses associated with the physical parameterizations and the surface pressure. From these two-dimensional fields, we evaluate the AAM budget and verifies that, for the three components, it is very well closed.

[11] We also extract the same fields from the ECMWF operational analysis every 3 hours for the calendar years 2002 and 2003, and for the NCEP reanalysis every 6 hours for the same calendar years. Note that in those two data sets, the surface stresses are produced by short-range forecast, yielding in part to the inconsistencies between the AAM approach and the torque approach noted in section 1.

[12] From these different sets of data, we extract a "mean day", computed by averaging the value at each given hour of the output on an integer number of years: 2 years for NCEP and ECMWF (2002–2003), and one "climatological year" for the LMD.

[13] At these frequency, we do not use the inverted barometer approximation to correct geodetic forcing for a

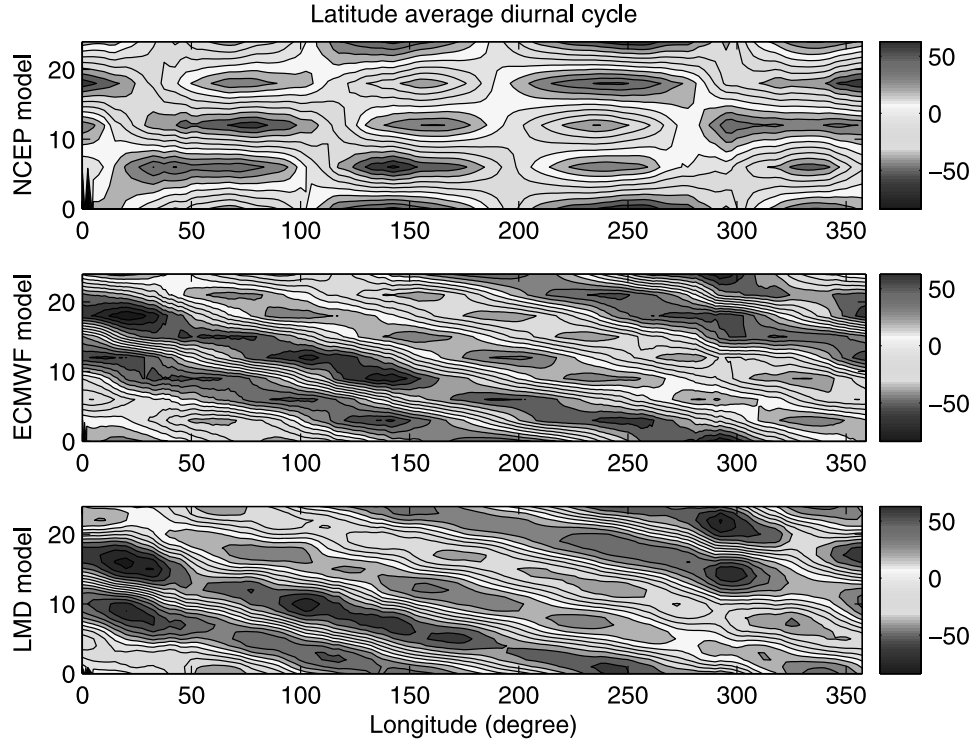

Figure 1. Latitude averaged pressure variation (in Pa) for the three models. The *y* axis is the time of the day, in hours. See color version of this figure at back of this issue.

static ocean response, as it is accepted to be only valid at periods for which the ocean has time to readjust, i.e., periods longer than a few days [see *Munk and McDonald*, 1960].

[14] The axe system is defined as follows: the Z axis is along the Earth mean rotation axis, the X axis is in the mean equatorial plan, and pointing to the Greenwich meridian, and the Y axis is at 90 degrees from the X axis in the mean equatorial plane. In this system, the LOD variation are associated with AAM variations and torques in the Z component and the polar motion and nutation with the X and Y components of AAM and torques.

3. Diurnal Cycle in Pressure and Barotropic Wind and Its Subharmonics

[15] The atmospheric mass distribution affects the angular momentum, which is estimated from the surface pressure field. The motion term is estimated from the barotropic wind. In this section, we discuss the pattern of the S_1 and S_2 waves in the pressure and barotropic wind fields.

[16] In Figure 1, we show the variation, for the mean day, of the surface pressure average over the latitude (with a $\cos\phi$ weighting). The amplitude and phase of the three models are fairly close, considering the different time resolutions of the models. Note that the NCEP, with 6 hourly data, is unable to catch the regular westward propagation of the wave, and simply show a standing wave with 6 hourly period. Animation 1 shows the same evolution for the three models on the mean day, in two dimensions.

[17] The diurnal tide is essentially a nonmigrating signal, with much larger values over continents than over oceans, and especially at low latitudes over Africa and Northern South America (see Animation 2). At other times it also has less pronounced maxima over the Tibetan Plateau, and Australia, i.e., again over high or/and desert terrain. Those maxima are also realistic with values around 1–1.5 mbar [see, e.g., *Dai and Wang*, 1999], and the phase is also correct, in the sense that the maximum amplitudes grossly occur at each places over continent between 0800 and 1200 local solar time (not shown). The rather noisy nonpropagating character of the diurnal pattern in surface pressure, is consistent with the fact that this signal is forced near the ground by the geographical inhomogeneities in the water vapor distribution, latent heating and sensible heat flux [see, e.g., *Hagan and Forbes*, 2002].

[18] The semidiurnal signal on surface pressure is dominated by an equatorially trapped planetary-scale migrating pattern of zonal wave number 2 in agreement with observations [*Dai and Wang*, 1999]. In amplitude its maximum at the equator is near 1.2 hPa, and its phase is such that a maximum is at the Greenwich Meridian near 1100 UT, those two values are also rather realistic. The rather smooth and propagating character of the semidiurnal pattern is consistent with the fact that it is forced by the absorption of the short-wave solar radiation by Ozone mainly in the stratosphere, and by water vapor in the troposphere. This wave was first estimated from ground measurement, and more recently, *Ponte and Ray* [2002] have estimated it by an interpolation of the ECMWF data, using a method proposed by *Van den Dool et al.* [1997].

[19] In order to be associated with AAM matter term variations, the pressure field has to present particular

Table 1. Surface Pressure Spherical Harmonics Coefficients for the S_1 Wave and the Three Models[a]

		M										
	Model	0	1	2	3	4	5	6	7	8	9	10
$\ell = 1$	NCEP	6 *100°*	19 *89°*									
			22 *10°*									
	ECMWF	3 *18°*	19 *132°*									
			22 *51°*									
	LMD	5 *78°*	19 *93°*									
			18 *16°*									
$\ell = 2$	NCEP	12 *−45°*	3 *48°*	8 *76°*								
			5 *49°*	11 *77°*								
	ECMWF	10 *−32°*	2 *72°*	8 *123°*								
			4 *76°*	10 *119°*								
	LMD	12 *−58°*	5 *19°*	10 *88°*								
			5 *78°*	12 *85°*								
$\ell = 3$	NCEP	14 *−108°*	15 *−97°*	4 *166°*	10 *2°*							
			16 *173°*	5 *139°*	8 *118°*							
	ECMWF	12 *−74°*	14 *−63°*	4 *165°*	7 *16°*							
			13 *−145°*	4 *142°*	6 *120°*							
	LMD	12 *−106°*	17 *−83°*	6 *143°*	12 *6°*							
			13 *166°*	6 *145°*	11 *128°*							
$\ell = 4$	NCEP	11 *140°*	5 *−156°*	5 *−106°*	7 *169°*	5 *158°*						
			5 *−110°*	5 *−116°*	9 *165°*	6 *99°*						
	ECMWF	7 *−179°*	2 *−94°*	4 *−77°*	7 *−133°*	4 *−162°*						
			6 *−29°*	4 *−136°*	9 *−155°*	9 *122°*						
	LMD	13 *137°*	5 *−163°*	6 *−102°*	10 *−170°*	1 *63°*						
			4 *−46°*	8 *−150°*	11 *−165°*	15 *106°*						
$\ell = 5$	NCEP	11 *81°*	4 *52°*	3 *−3°*	5 *−136°*	4 *124°*	10 *166°*					
			4 *−64°*	3 *43°*	6 *−129°*	6 *−52°*	12 *85°*					
	ECMWF	13 *129°*	5 *76°*	3 *50°*	5 *−97°*	2 *−144°*	6 *−133°*					
			5 *−54°*	1 *−42°*	6 *−102°*	5 *−3°*	8 *139°*					
	LMD	8 *62°*	11 *102°*	5 *−14°*	4 *−157°*	4 *162°*	12 *−175°*					
			6 *−29°*	2 *−64°*	8 *−123°*	9 *−14°*	13 *121°*					
$\ell = 6$	NCEP	11 *−33°*	4 *−36°*	3 *−14°*	7 *−43°*	4 *135°*	9 *86°*	7 *158°*				
			5 *158°*	5 *−67°*	3 *−40°*	1 *−102°*	11 *−51°*	3 *−28°*				
	ECMWF	8 *28°*	2 *37°*	3 *55°*	7 *−6°*	2 *−168°*	5 *134°*	5 *−133°*				
			6 *−146°*	2 *−6°*	0 *68°*	2 *−6°*	10 *8°*	2 *21°*				
	LMD	10 *−14°*	4 *19°*	7 *15°*	10 *−24°*	4 *−170°*	8 *123°*	10 *−172°*				
			5 *−157°*	4 *1°*	3 *−64°*	7 *−66°*	13 *−13°*	5 *100°*				
$\ell = 7$	NCEP	7 *−128°*	3 *−176°*	5 *−121°*	3 *−34°*	3 *152°*	4 *−22°*	3 *−4°*	5 *165°*			
			1 *72°*	2 *−157°*	4 *66°*	4 *49°*	3 *169°*	4 *−161°*	4 *−53°*			
	ECMWF	9 *−110°*	3 *−154°*	3 *−96°*	3 *22°*	3 *−151°*	5 *71°*	4 *40°*	5 *−130°*			
			4 *139°*	3 *153°*	4 *111°*	2 *101°*	1 *105°*	5 *−153°*	3 *37°*			
	LMD	7 *−150°*	4 *−90°*	1 *137°*	8 *−39°*	5 *−103°*	5 *17°*	4 *26°*	4 *−109°*			
			4 *160°*	2 *122°*	4 *54°*	4 *153°*	6 *−95°*	4 *−157°*	2 *−37°*			
$\ell = 8$	NCEP	11 *−177°*	2 *121°*	5 *131°*	2 *108°*	3 *−79°*	3 *−87°*	3 *5°*	4 *−15°*	3 *−153°*		
			2 *−30°*	6 *85°*	0 *−73°*	3 *47°*	5 *93°*	2 *152°*	2 *−114°*	4 *−71°*		
	ECMWF	7 *−107°*	2 *−172°*	5 *−157°*	3 *144°*	1 *−26°*	2 *−6°*	2 *100°*	4 *57°*	2 *−69°*		
			2 *57°*	3 *165°*	2 *43°*	1 *69°*	3 *177°*	2 *−120°*	1 *−167°*	3 *−9°*		
	LMD	8 *−147°*	3 *−116°*	9 *−171°*	2 *120°*	2 *−76°*	4 *−63°*	4 *12°*	3 *−5°*	5 *−70°*		
			2 *30°*	3 *163°*	5 *59°*	5 *100°*	8 *142°*	5 *−156°*	4 *−134°*	5 *−93°*		
$\ell = 9$	NCEP	7 *−8°*	2 *−18°*	3 *90°*	4 *113°*	2 *70°*	3 *130°*	3 *−57°*	5 *122°*	5 *62°*	5 *83°*	
			3 *−96°*	4 *−98°*	2 *−32°*	2 *107°*	2 *−18°*	1 *125°*	2 *72°*	1 *68°*	1 *−123°*	
	ECMWF	5 *67°*	7 *−27°*	0 *151°*	1 *−156°*	2 *135°*	3 *−138°*	3 *−6°*	3 *−162°*	5 *125°*	1 *121°*	
			2 *−76°*	3 *−47°*	2 *−1°*	1 *148°*	1 *−116°*	0 *−115°*	1 *134°*	3 *130°*	3 *−101°*	
	LMD	3 *33°*	1 *−64°*	3 *−129°*	6 *143°*	5 *98°*	5 *148°*	3 *−17°*	2 *178°*	6 *136°*	1 *−48°*	
			2 *−45°*	3 *−59°*	2 *−142°*	2 *81°*	5 *74°*	3 *88°*	4 *117°*	2 *−173°*	3 *174°*	
$\ell = 10$	NCEP	7 *55°*	2 *−44°*	4 *−22°*	2 *148°*	2 *113°*	1 *−21°*	1 *48°*	3 *104°*	3 *26°*	3 *−33°*	2 *126°*
			1 *−156°*	3 *−87°*	2 *−178°*	2 *−128°*	1 *132°*	2 *−76°*	2 *60°*	3 *−26°*	3 *104°*	1 *14°*
	ECMWF	7 *92°*	1 *−145°*	4 *3°*	3 *−130°*	1 *137°*	2 *−102°*	1 *13°*	3 *177°*	2 *26°*	2 *46°*	1 *−154°*
			3 *−39°*	3 *−33°*	1 *−4°*	1 *46°*	2 *−177°*	1 *−122°*	2 *107°*	2 *32°*	2 *176°*	2 *−107°*
	LMD	4 *100°*	2 *−1°*	6 *−9°*	3 *−142°*	3 *84°*	3 *81°*	2 *87°*	2 *130°*	3 *65°*	3 *100°*	2 *−78°*
			3 *−115°*	1 *−72°*	4 *−139°*	1 *−139°*	2 *−84°*	6 *−2°*	4 *62°*	2 *−4°*	4 *140°*	1 *−164°*

[a]The surface pressure spherical harmonics coefficients are in Pa. The first number is the amplitude of the wave and the second gives the phase (lag in hours). The first row of each model is the real part of the spherical harmonics (in cos $m\lambda$), and the second row is the imaginary part (in sin $m\lambda$). The phase (in italics) is given in hours with respect to 0000 UT.

geographical patterns: the Earth rotation speed is affected only if the inertia of the atmosphere along the mean rotation axis changes, which, in terms of spherical harmonics, is a degree 2 order zero. The polar motion will only be affected by distribution of degree 2 order 1, and the geocenter motion by degree 1 order 0 the Z axis, and by degree 1 order 1 for the X and Y axes.

Table 2. Surface Pressure Spherical Harmonics Coefficients for the S_2 Wave and the Three Models[a]

		M									
	Model	0	1	2	3	4	5	6	7	8	9	10
$\ell = 1$	ECMWF	3 *−128°*	3 *126°*									
			2 *87°*									
	LMD	0 *26°*	2 *101°*									
			2 *15°*									
$\ell = 2$	ECMWF	23 *52°*	2 *98°*	67 *24°*								
			4 *−139°*	64 *−67°*								
	LMD	9 *−65°*	2 *17°*	58 *−43°*								
			2 *−179°*	56 *−134°*								
$\ell = 3$	ECMWF	7 *55°*	2 *−81°*	3 *22°*	5 *42°*							
			1 *−130°*	3 *47°*	5 *50°*							
	LMD	3 *14°*	2 *−36°*	4 *−5°*	5 *−88°*							
			1 *119°*	2 *−65°*	7 *−46°*							
$\ell = 4$	ECMWF	11 *−131°*	1 *−167°*	14 *−159°*	2 *45°*	3 *−78°*						
			2 *46°*	14 *115°*	1 *−116°*	2 *45°*						
	LMD	5 *81°*	1 *−175°*	18 *136°*	2 *56°*	3 *−53°*						
			1 *11°*	18 *49°*	1 *−135°*	5 *51°*						
$\ell = 5$	ECMWF	3 *−61°*	2 *50°*	1 *−128°*	1 *129°*	3 *101°*	2 *70°*					
			2 *−111°*	3 *−103°*	2 *−128°*	2 *109°*	1 *14°*					
	LMD	0 *−117°*	1 *157°*	1 *45°*	3 *69°*	1 *92°*	2 *14°*					
			1 *−140°*	2 *−102°*	1 *110°*	1 *34°*	1 *−14°*					
$\ell = 6$	ECMWF	3 *34°*	2 *26°*	2 *−74°*	2 *−103°*	1 *−115°*	2 *−5°*	4 *102°*				
			0 *−118°*	0 *60°*	1 *152°*	1 *72°*	0 *−69°*	2 *7°*				
	LMD	0 *−108°*	1 *102°*	2 *−47°*	1 *−163°*	1 *156°*	1 *−48°*	2 *59°*				
			1 *112°*	3 *−111°*	1 *−131°*	0 *95°*	0 *−126°*	1 *−77°*				
$\ell = 7$	ECMWF	4 *162°*	1 *−95°*	1 *49°*	2 *−73°*	2 *−113°*	1 *−3°*	2 *−24°*	1 *105°*			
			2 *100°*	0 *23°*	1 *34°*	2 *6°*	1 *−134°*	2 *−105°*	2 *−50°*			
	LMD	0 *28°*	1 *107°*	1 *−108°*	2 *−116°*	1 *−145°*	0 *−74°*	2 *−36°*	2 *50°*			
			1 *79°*	1 *107°*	0 *−135°*	1 *66°*	1 *−10°*	1 *−120°*	1 *−87°*			
$\ell = 8$	ECMWF	5 *59°*	0 *−147°*	2 *104°*	1 *−32°*	2 *99°*	1 *134°*	1 *−112°*	1 *−107°*	1 *135°*		
			2 *54°*	1 *38°*	2 *2°*	1 *−46°*	2 *54°*	1 *141°*	1 *−174°*	1 *−56°*		
	LMD	1 *−99°*	1 *88°*	1 *6°*	1 *−20°*	0 *−138°*	0 *86°*	1 *−157°*	0 *−132°*	1 *81°*		
			1 *−73°*	0 *24°*	0 *1°*	1 *53°*	1 *10°*	0 *118°*	1 *120°*	1 *−130°*		
$\ell = 9$	ECMWF	1 *128°*	1 *143°*	1 *90°*	1 *55°*	1 *91°*	1 *93°*	2 *36°*	1 *−28°*	2 *−35°*	1 *−109°*	
			0 *−152°*	0 *−119°*	1 *29°*	1 *−93°*	2 *112°*	1 *−140°*	1 *−178°*	0 *−160°*	2 *151°*	
	LMD	1 *−148°*	0 *−106°*	1 *129°*	1 *56°*	1 *10°*	1 *44°*	1 *149°*	1 *−174°*	0 *−149°*	1 *−136°*	
			1 *−84°*	1 *79°*	1 *11°*	0 *1°*	1 *−96°*	1 *25°*	1 *122°*	1 *105°*	1 *93°*	
$\ell = 10$	ECMWF	4 *−108°*	1 *33°*	1 *−15°*	1 *−121°*	1 *−163°*	1 *60°*	0 *−138°*	1 *−155°*	0 *23°*	1 *37°*	1 *143°*
			2 *75°*	1 *−109°*	1 *−92°*	1 *−119°*	1 *−67°*	1 *−71°*	0 *89°*	0 *59°*	1 *−93°*	2 *119°*
	LMD	1 *102°*	1 *−84°*	1 *−143°*	1 *149°*	1 *88°*	1 *20°*	1 *35°*	0 *−151°*	0 *6°*	0 *28°*	1 *127°*
			0 *60°*	1 *−165°*	1 *50°*	0 *33°*	1 *−125°*	2 *−91°*	0 *146°*	1 *15°*	1 *−24°*	1 *92°*

[a]The surface pressure spherical harmonics coefficients are in Pa. The first number is the amplitude of the wave and the second gives the phase (lag in hours). The first row of each model is the real part of the spherical harmonics (in cos $m\lambda$), and the second row is the imaginary part (in sin $m\lambda$). The phase (in italics) is given in hours with respect to 0000 UT.

[20] To allow a thorough comparison, Tables 1, 2, and 3 give the spherical harmonic decomposition of the surface pressure for the waves S_1, S_2, S_3, and S_4 for the ECMWF and LMD model. In Tables 1, 2, and 3, we go up to degree 10, to allow comparison with the coefficients used in the dealiasing of the spatial gravity missions as GRACE or CHAMP. The coefficients are quite similar for the S_1 waves from the NCEP reanalysis and LMD model, and the values from the ECMWF analysis present phase differences at the level of some tens of degree.

[21] As well known from *Chapman and Lindzen* [1970], for instance, the S_2 wave is dominated by a degree 2 order 2 wave, and S_1 by a degree 1 order 1 wave. In Tables 1 and 2, note that this part of the signal is fairly consistent from one model to another. The part of the signal relevant for Earth rotation (degree 2 order 0 and 1) is quite smaller, and differs to a large extend from one model to the other, which implies a tiny (and not very reliable) effect on the Earth rotation.

[22] The barotropic wind, shown in Figure 2, present similarities between S_1 and S_2: it is dominated by a convergence-divergence field at global scale, but with two convergence points (and two divergence points) for S_2 and only one for S_1. Additionally, the size of the S_2 wind signal does not reflect the ocean-continent distribution, as it is the case for the S_1 wave.

[23] Again, this wind distribution is inefficient to generate a variation in Earth rotation: the motion term of the angular momentum is associated with the mean rotation of the atmosphere, which correspond to the rotational part of the wind field. A purely divergent field has no rotation part, so the wind term is small as well. It will be smaller for the S_2 wave than for the S_1 wave, because the ocean-continent distribution perturbs the purely divergent field for S_1 and not for S_2.

[24] Consequently, using only the pattern in the pressure and wind field, we can expect the effect on Earth rotation to be small, and even smaller for S_2 than for S_1 and not very consistent from one model to another. We can also expect a larger and more consistent effect on the equatorial geocenter motion. Even if there is a large diurnal and semidiurnal

Table 3. Surface Pressure Spherical Harmonics Coefficients for the S_3 Wave and the Three Models[a]

		M									
	Model	0	1	2	3	4	5	6	7	8	9	10
$\ell = 1$	ECMWF	0 −114°	1 −90°									
			0 162°									
	LMD	0 −80°	0 −108°									
			0 108°									
$\ell = 2$	ECMWF	2 98°	0 96°	1 −71°								
			0 −66°	1 −115°								
	LMD	0 59°	0 −132°	0 −95°								
			0 96°	0 −119°								
$\ell = 3$	ECMWF	0 148°	1 −119°	1 32°	3 −178°							
			4 −74°	1 −97°	1 58°							
	LMD	0 −85°	0 75°	0 −91°	1 −4°							
			1 63°	0 −162°	1 −76°							
$\ell = 4$	ECMWF	1 147°	1 93°	1 116°	2 165°	1 −75°						
			1 164°	1 55°	1 178°	1 −133°						
	LMD	1 14°	0 −57°	1 −136°	3 80°	2 161°						
			1 95°	2 −72°	4 139°	1 117°						
$\ell = 5$	ECMWF	1 −61°	1 29°	1 −69°	2 −161°	1 31°	2 176°					
			1 160°	0 22°	3 138°	1 −103°	2 75°					
	LMD	1 40°	0 102°	0 −142°	1 −154°	1 −137°	1 −102°					
			1 91°	0 152°	0 −138°	0 −42°	0 −90°					
$\ell = 6$	ECMWF	0 −84°	1 −135°	0 −92°	1 −21°	0 −9°	1 66°	1 −150°				
			1 82°	0 −23°	2 −84°	1 −41°	1 −64°	0 122°				
	LMD	1 −169°	0 69°	0 35°	1 −109°	1 −88°	1 −92°	1 −130°				
			0 163°	1 83°	0 3°	1 −127°	0 −125°	0 63°				
$\ell = 7$	ECMWF	0 123°	1 −138°	1 165°	0 −140°	0 162°	3 −7°	1 111°	1 −25°			
			0 169°	0 74°	1 −37°	1 101°	2 72°	1 −160°	2 −42°			
	LMD	0 −138°	0 −149°	0 2°	0 43°	0 6°	0 16°	0 123°	1 −134°			
			1 −128°	0 −75°	1 24°	0 −108°	0 −117°	0 28°	1 66°			
$\ell = 8$	ECMWF	1 117°	0 58°	1 97°	1 71°	1 126°	1 87°	0 39°	0 −179°	1 −81°		
			0 173°	0 −175°	1 112°	1 117°	0 133°	0 −175°	0 −134°	0 −110°		
	LMD	1 −1°	0 −161°	0 −143°	0 134°	1 70°	0 17°	1 21°	0 114°	1 −141°		
			0 −76°	0 −120°	0 −111°	1 −2°	0 −107°	0 −162°	1 43°	0 101°		
$\ell = 9$	ECMWF	0 −141°	2 111°	0 −70°	1 109°	0 114°	0 109°	0 112°	0 101°	0 26°	1 −84°	
			0 −79°	1 −68°	0 −96°	1 −91°	1 113°	0 130°	0 71°	0 65°	0 −126°	
	LMD	0 56°	0 −14°	0 −130°	0 −110°	0 45°	0 154°	0 −37°	0 34°	0 83°	0 −152°	
			0 −3°	0 105°	0 178°	0 −15°	0 −23°	0 −146°	1 −126°	0 −162°	0 −49°	
$\ell = 10$	ECMWF	1 −93°	0 −81°	1 89°	0 −6°	0 82°	0 −135°	0 −101°	1 98°	0 105°	0 151°	0 −56°
			1 131°	0 110°	0 −53°	0 −110°	0 118°	0 15°	0 115°	0 72°	0 86°	0 111°
	LMD	0 −159°	0 10°	0 15°	0 −22°	0 −125°	0 153°	1 175°	0 −87°	0 8°	0 59°	0 110°
			0 4°	0 51°	0 72°	0 159°	0 26°	0 58°	0 −83°	0 −132°	0 −176°	0 −102°

[a]The surface pressure spherical harmonics coefficients are in Pa. The first number is the amplitude of the wave and the second gives the phase (lag in hours). The first row of each model is the real part of the spherical harmonics (in cos $m\lambda$), and the second row is the imaginary part (in sin $m\lambda$). The phase (in italics) is given in hours with respect to 0000 UT.

signal in the atmosphere, the effect on the Earth rotation is expected to be small.

4. Diurnal Angular Momentum Budget of the Atmosphere and Earth Rotation

4.1. AAM Budget in the LMD-GCM

[25] The angular momentum budget equation is given by

$$\frac{d\mathbf{H}_{\text{mass}}}{dt} + \frac{d\mathbf{H}_{\text{wind}}}{dt} + \boldsymbol{\Omega} \wedge (\mathbf{H}_{\text{mass}} + \mathbf{H}_{\text{wind}}) = \boldsymbol{\Gamma}_{\text{Ellips}} + \boldsymbol{\Gamma}_{\text{Mount}} + \boldsymbol{\Gamma}_{\text{Fric}} + \boldsymbol{\Gamma}_{\text{Grav W}} \quad (1)$$

where the time derivative are computed in the Earth fixed reference frame and $\boldsymbol{\Omega}$ is the Earth rotation vector. The expression for computing the different torques and the angular terms has been published in several studies, such as those by *Barnes et al.* [1983], *Wahr* [1982], and *de Viron et al.* [2001], and we will not repeat them here.

[26] Figure 3 shows the AAM time derivative and the total torque for the "mean day" from the three models. It can be observed that the angular momentum budget equations are well closed in the LMD model and not in the reanalyses. Note also that both the AAM time derivatives and the torques differ strongly from one data set to the other. Consequently, in this study, we will next focus on the GCM LMDz results only. It does not mean that the results are closer to reality, but we can only investigate the angular momentum budget if it is reasonably well closed. Note nevertheless that as our model has realistic tides (see section 3), we can nevertheless expect that the results from the GCM LMDz will be relevant for the real atmosphere.

[27] Figure 4 shows the angular momentum budget for S_1, S_2, and S_3 from the LMD model, for the three components, and using a phasor plot representation (the X component is the AAM budget closure in phase with the civil time, and the Y component is the AAM budget in quadrature). This representation allows to visualize directly the relative amplitude of the different terms in this budget, and to discuss

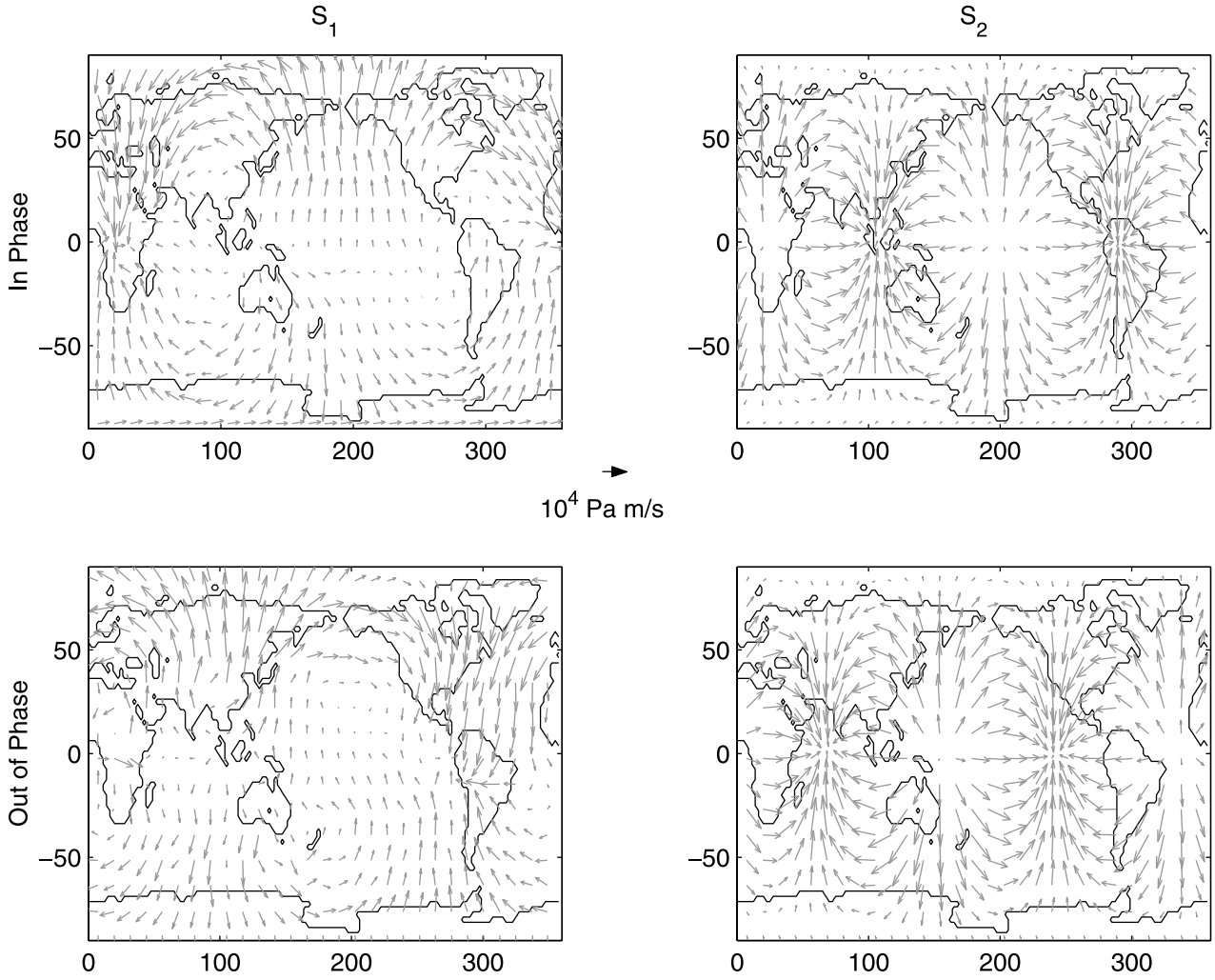

Figure 2. Barotropic wind for S_1 and S_2 in the LMD model.

their relative importance. The first observation that can be done is that the contribution from the mass term and wind term tends to cancel each other, for the three components and for the three waves. It means again that we need a good precision in order to compare the AAM terms, the total AAM being a residual between two large contributors.

[28] For the X component, the ellipsoidal torque dominates, but not as strongly as at synoptic timescale, for which the mountain torque is very small [see *de Viron et al.*, 1999]. For the Y component, S_1 produce a large ellipsoidal torque, most of it being cancelled by the other torques.

[29] As, for the diurnal torque, the dynamics at regional scale is very important (mostly for the mountain torque), it is important to localize where the interaction occurs, which is possible by integrating on every continent and ocean separately. As explain in previous studies [e.g., *de Viron et al.*, 2001], the mountain torque results from the product of the surface pressure by the topography derivative, only the longitude derivative being relevant for the Z component, and both longitude and latitude derivative for the equatorial components. In that paper, Antarctica was said to be dominant for the equatorial component, in the time domain. Of course, this is not expected to be the case for the diurnal cycle, as those high latitude only present a small, if any, diurnal cycle in the surface pressure. In our study, we find the Asia (Himalaya) to be, by far, the major contributor for the equatorial exchange of angular momentum, with some effect, mostly in the Y component, of the South America. For the axial torque, the Asia and South America dominates the exchange, which is not surprising considering the longitude derivative of the topography, as shown in Figure 1 of *de Viron et al.* [2001], for instance. The major contributions from the friction torque occur over the same continents: Asia and South America. The same is also true for the gravity wave drag torque, with an additional noticeable contribution from Africa in the diurnal torque.

4.2. Equatorial AAM Budget at Diurnal Period

[30] When studying the effect on Earth rotation, it makes sense to look at the budget in terms of prograde and retrograde waves. The prograde diurnal in the Earth reference frame will be associated with high-frequency polar motion, and the retrograde diurnal will be associated with nutation. Mathematically, it is equivalent to decompose an elliptic motion (periodic motion of different amplitude in X and Y) into two circular motions, one in the same direction as the Earth rotation and one in the opposite direction. The mathematical expression to use are given, for instance, by

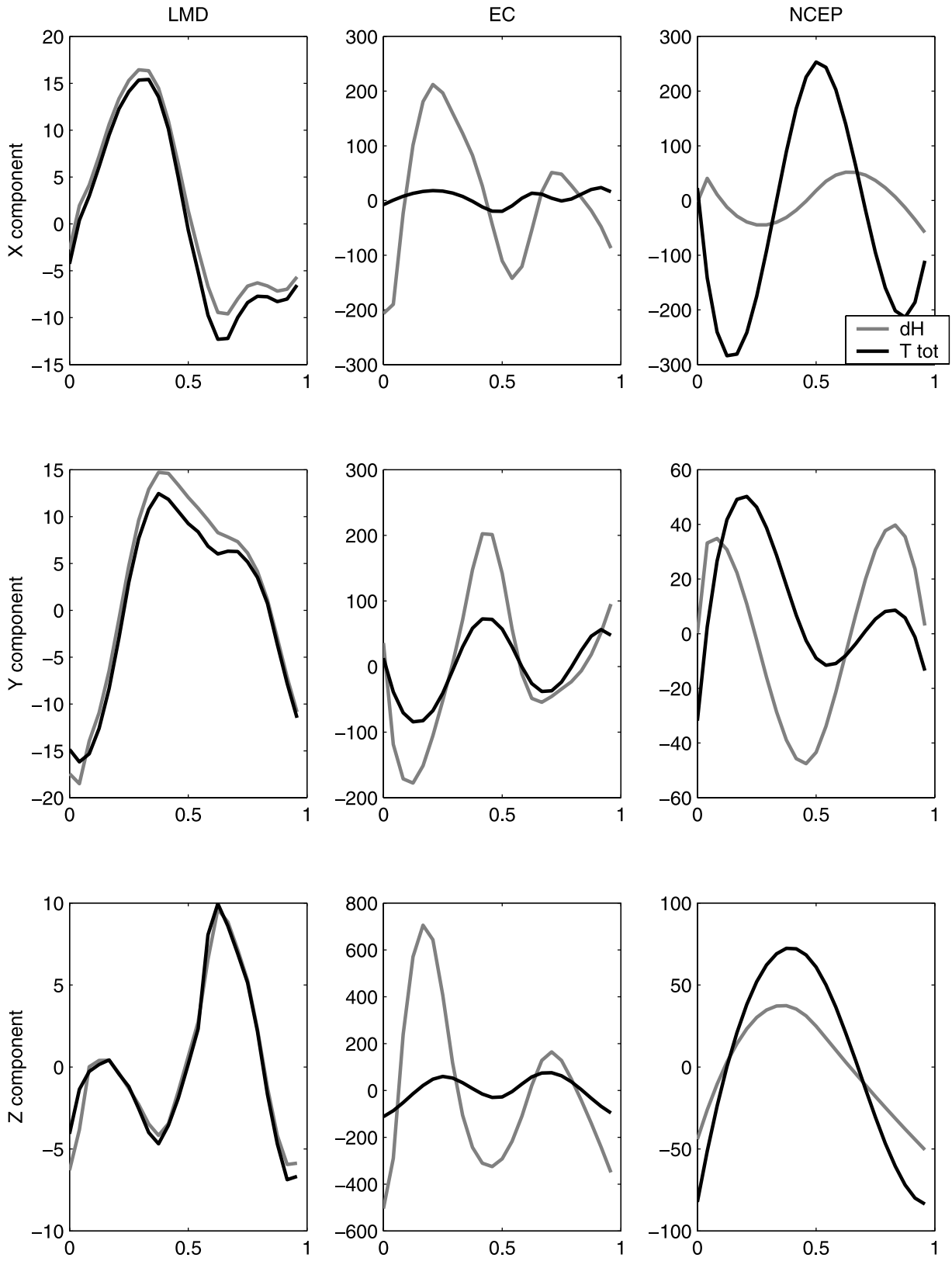

Figure 3. Angular momentum budget equation for the three models (unit hadleys, i.e., 10^{18} N m). The NCEP and EC results have been interpolated using their harmonics development.

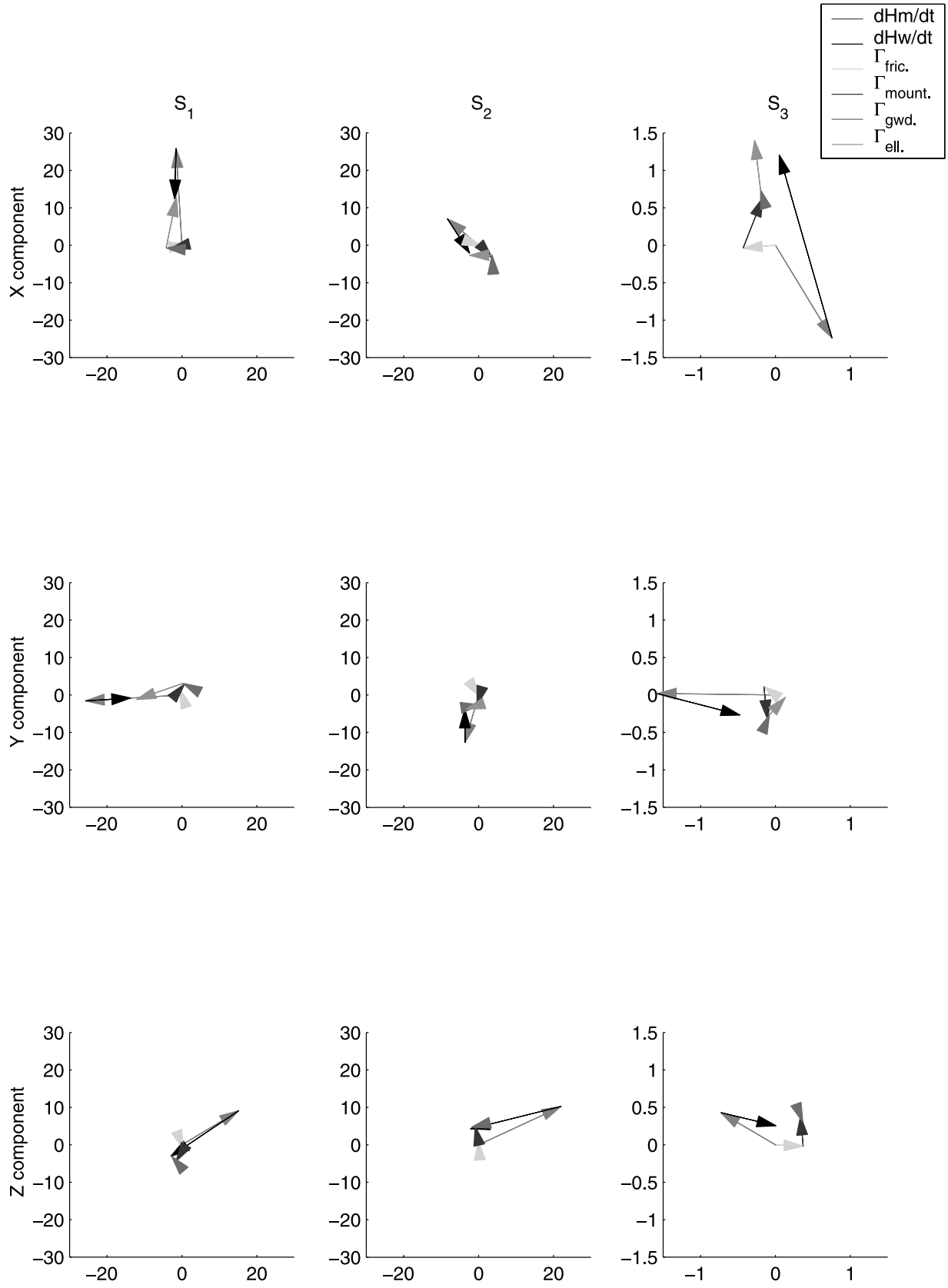

Figure 4. Phasor plot of the angular momentum budget, the phase is with respect to 0000 UT (unit hadleys, i.e., 10^{18} N m). The *X* component is the AAM budget closure in phase with the civil time, and the *Y* component is the AAM budget in quadrature. See color version of this figure at back of this issue.

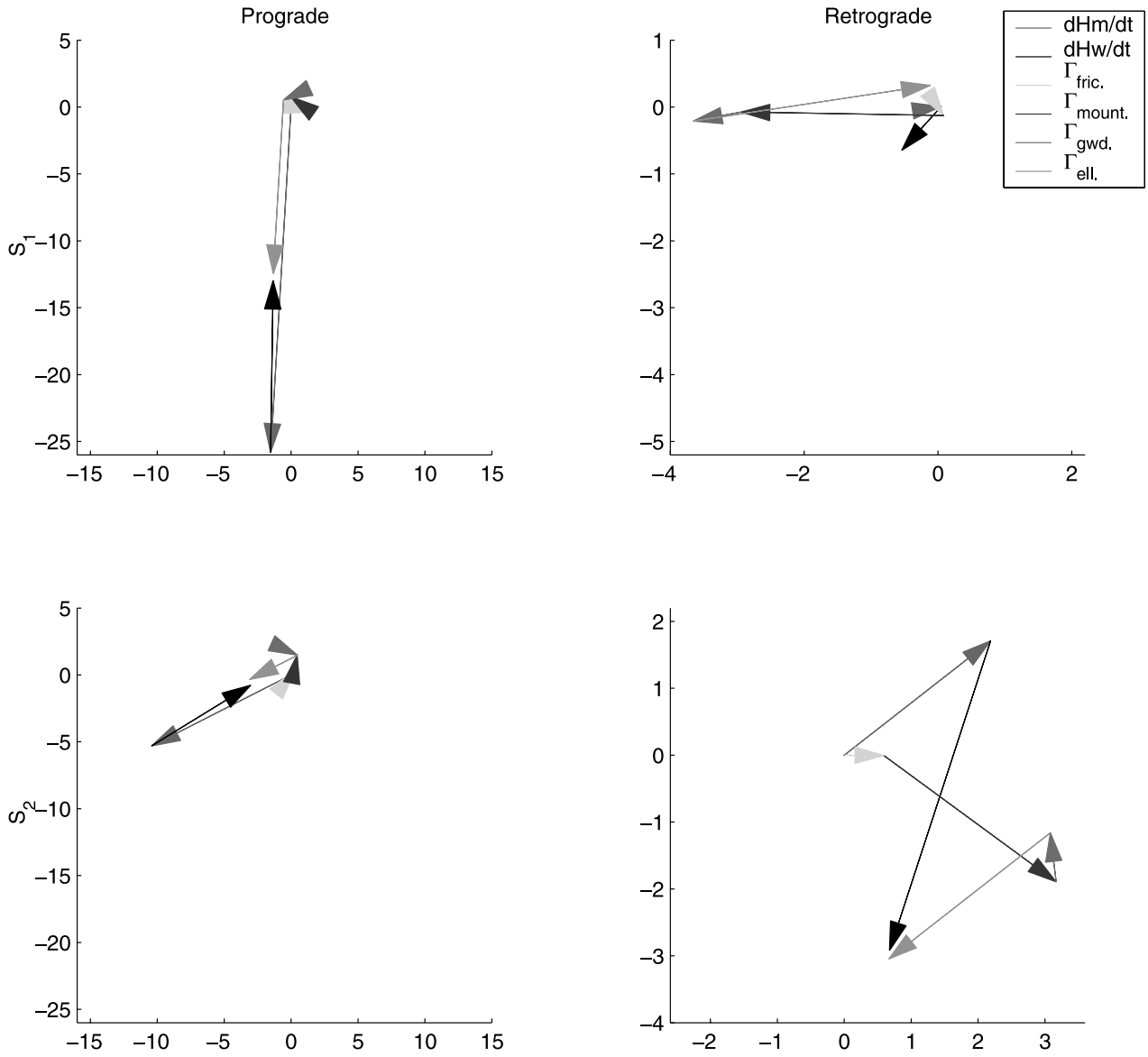

Figure 5. Phasor plot of the equatorial angular momentum budget expressed in terms of prograde and retrograde terms, the phase is with respect to 0000 UT (unit hadleys, i.e., 10^{18} N m). See color version of this figure at back of this issue.

Dehant et al. [1996]. Figure 5 shows the AAM budget for the equatorial components, decomposed in prograde and retrograde terms. Again, the angular momentum budget is fairly well closed, with the retrograde wind term larger than the equivalent matter term (by an order of magnitude for S_1 and by a factor of 2 for S_2). This last results is consistent with other studies [see, e.g., *Bizouard et al.*, 1998]. In Figure 5, note as well that the diurnal retrograde ellipsoidal torque is near exactly cancelled by the other torques, the total torque being at the level of 10% of the ellipsoidal torque. This confirms the hypothesis made by *de Viron et al.* [2001] and *Marcus et al.* [2004] that such a balance was the necessary condition to close the AAM budget in the retrograde diurnal frequency band. Nevertheless, note that, in the model, the friction torque contribution is substantially smaller than the mountain torque, which was not the case in the NCEP reanalysis by *de Viron et al.* [2001] and *Marcus et al.* [2004]. The prograde component does not have the same dynamic constraint as the retrograde, and the ellipsoidal torque dominates strongly the others as shown on Figure 5.

4.3. Impact on the Earth Orientation Parameters

[31] In the LMD-GCM, the torque and the angular momentum approach are equivalent, as the angular momentum budget equation is verified. Consequently, we will use the angular momentum approach to evaluate the Earth rotation effect. Table 4 gives the Earth rotation effect, for the S_1, S_2, and S_3 waves (when meaningful) for the three models. As expected from the results in section 4.1, the amplitude and phase of the effect, according to the different models, are very different. For the S_1 polar motion, there is a reasonable agreement in amplitude and phase between the results from the NCEP model and from the LMD model. The ECMWF results differ both in amplitude (nearly a factor 5) and in phase. This difference between the ECMWF results and the LMD results also appear for the higher

Table 4. Diurnal and Subdiurnal Effect on the Earth Rotation[a]

	Polar Motion X			Polar Motion Y			LOD Variations		
	LMD	ECMWF	NCEP	LMD	ECMWF	NCEP	LMD	ECMWF	NCEP
S_1	188, *−2.7*	390, *−1.9*	121, *−2.4*	231, *−1.8*	1084, *−1.8*	196, *−2.3*	2, *9.5*	29, *−3.9*	5, *−6.00*
S_2	1, *3.1*	13, *1.32*		1, *1.8*	10, *−2.0*		1, *−11.1*	35, *−9.6*	
S_3	0.1, *0.2*	1, *1.9*		0	0.3, *0.4*		0	9, *5.1*	

[a]The amplitude of the polar motion is given in μas and of the LOD variation in μs. The phase (in italics) is given in hours with respect to 0000 UT.

frequencies. At the S_1 frequency, the size of the polar motion is at the level of 0.2 milliarc second (mas) (according to the LMD and NCEP model) or 1 mas (according to the ECMWF). Without additional information, it is difficult to determine which among these data sets gives the right answer, if any.

4.4. Diurnal and Subdiurnal Geocenter Displacement

[32] The position of the geometrical center of the terrestrial reference frame, i.e., position of the crust, with respect to the center of mass of the Earth is given by

$$\begin{aligned} x_{CM} &= \frac{a^3}{M_T}\left(1+\frac{M_L}{M_T}\frac{h_1+2l_1}{3}\right)\int_S \Delta\sigma \sin^2\theta\cos\lambda\, d\theta d\lambda, \\ y_{CM} &= \frac{a^3}{M_T}\left(1+\frac{M_L}{M_T}\frac{h_1+2l_1}{3}\right)\int_S \Delta\sigma \sin^2\theta\sin\lambda\, d\theta d\lambda, \\ z_{CM} &= \frac{a^3}{M_T}\left(1+\frac{M_L}{M_T}\frac{h_1+2l_1}{3}\right)\int_S \Delta\sigma \sin\theta\cos\theta\, d\theta d\lambda, \end{aligned} \quad (2)$$

where a is the Earth mean radius, M_T is the mass of the Earth, M_L is the total mass of the load, h_1 and l_1 are the load Love number, as defined by *Farrell* [1972], and $\Delta\sigma$ is the atmospheric mass distribution corresponding to the tidal wave. Table 5 gives the geocenter motion, for the S_1, S_2, and S_3 waves (when meaningful) for the three models.

[33] As shown in section 3, the diurnal pressure waves have a strong degree 1, order 1 spherical harmonic component, which is associated with a geocenter displacement in the equatorial plan.

[34] Note that, unlike for the Earth rotation, the diurnal geocenter signal is very similar from one model to the other. This signal is large, which is not surprising when considering the diurnal part of Figure 1, where the degree one pattern of the surface pressure distribution is very clear. This consistency between the models gives us much more confidence for the diurnal geocenter motion than for any of the other quantities we estimate here.

5. Conclusion

[35] In this study, we used three different atmospheric data sets to analyze the geodetic consequences of the diurnal and semidiurnal atmospheric tides. We show that the three models differ strongly, which is not surprising as they have different input data and different parameterization. Consequently, it is difficult to consider our results as more than orders of magnitude. Nevertheless, our analysis provides important qualitative insights on atmospheric effects on geodetic parameters at diurnal and subdiurnal timescale.

[36] First, we estimated the spherical harmonic decomposition of the surface pressure, and found differences between the LMD model and the NCEP reanalysis, on the one hand, and between the LMD model and the ECMWF analysis on the other hand. As this last model is used to dealias the GRACE data from the high-frequency signal, we advise caution for the diurnal cycle.

[37] We also used the LMD model (purely dynamical model, with no data assimilation) to study the angular momentum budget of the atmosphere at diurnal timescales. We confirm the assertion of *de Viron et al.* [2001] that the budget can only be closed in the diurnal retrograde band if the ellipsoidal torque is nearly exactly compensated by the local torque (here, mostly the mountain torque).

[38] We then investigate the effect on some geodetic observable, namely the Earth rotation variations (LOD variations and polar motion) and the geocenter motion. We show that the three models predict very different Earth rotation variations, both for diurnal and semidiurnal period. On the contrary, they predict quite similar geocenter motion at diurnal period. This difference comes from two different reasons.

[39] 1. The geocenter is only affected by change in the atmospheric pressure, whereas the wind term dominates the changes in Earth rotation. As the wind terms differ strongly from one model to another (to a larger extent than the mass term), the Earth rotation effects will also differ strongly.

[40] 2. Geometrically speaking, the diurnal and semidiurnal signal in the pressure and the wind are rather inefficient to create AAM variation. Consequently, the AAM changes come from the very small part of the wind and pressure field which has the right pattern. The opposite occurs for the diurnal geocenter motion: the S_1 pressure wave has the right geometry to generate geocenter motion;

Table 5. Diurnal and Subdiurnal Effect on the Geocenter[a]

	X			Y			Z		
	LMD	ECMWF	NCEP	LMD	ECMWF	NCEP	LMD	ECMWF	NCEP
S_1	0.70, *−0.2*	0.69, *−2.8*	0.70, *0.0*	0.65, *4.9*	0.82, *2.6*	0.83, *5.3*	0.09, *0.8*	0.05, *4.7*	0.11, *−0.7*
S_2	0.06, *−0.8*	0.11, *−2.4*		0.07, *5.0*	0.08, *0.2*		0	0.05, *−9.5*	
S_3	0	0.04, *−11.9*		0	0.01, *−4.8*		0	0	

[a]Effects in mm. The phase (in italic) is given in hours with respect to 0000 UT.

consequently, the dominant part of the signal (which is common from one model to another) is directly efficient. This results in a large and consistent geocenter motion. Even if S_2 is the larger signal in the subdiurnal band, its spherical harmonic of degree 2 and order 2 geometry prevents it to generate noticeable effects on the Earth orientation parameters or geocenter location. Indeed the LOD is affected by atmospheric patterns that are zonally symmetric, polar motion by spherical harmonics of degree 2 and order 1, and geocenter motion by patterns of zonal wave number 1, and the S_2 wave is dominated by a zonal wave number 2 structure. On the contrary, the S_1 waves has a signal large enough to create an observable signal in polar motion (at the level of 0.2 mas), and in the geocenter motion (1 mm). This last result is the more robust, as the data sets agree both in amplitude and in phase on the evaluation.

[41] **Acknowledgment.** The work of O. d. V. was financially supported by the Belgian Service Public fédéral de Programmation Politique scientifique.

References

Barnes, R. T. H., R. Hide, A. A. White, and C. A. Wilson (1983), Atmospheric angular momentum fluctuations, length-of-day changes and polar motion, *Proc. R. Soc. London, Ser. A*, *387*, 31–73.

Bizouard, C., A. Brzezinski, and S. Petrov (1998), Diurnal atmospheric forcing and temporal variations of the nutation amplitudes, *J. Geod.*, *72*, 561–577.

Chapman, S., and R. S. Lindzen (1970), *Atmospheric Tides*, *Thermal and Gravitational*, 200 pp., Springer, New York.

Dai, A., and J. Wang (1999), Diurnal and semidiurnal tides in global surface pressure fields, *J. Atmos. Sci.*, *56*, 3874–3891.

Dehant, V., C. Bizouard, J. Hinderer, H. Legros, and M. Lefftz (1996), On atmospheric pressure perturbations on precession and nutations, *Phys. Earth Planet. Inter.*, *96*, 25–39.

de Viron, O., C. Bizouard, D. Salstein, and V. Dehant (1999), Atmospheric torque on the Earth and comparison with atmospheric angular momentum variations, *J. Geophys. Res.*, *104*(B3), 4861–4876.

de Viron, O., S. L. Marcus, and J. O. Dickey (2001), Diurnal angular momentum budget of the atmosphere and its consequences for Earth's nutation, *J. Geophys. Res.*, *106*, 26,747–26,759.

Farrell, W. E. (1972), Deformation of the Earth by surface load, *Rev. Geophys.*, *10*, 761–797.

Hagan, M. E. (1996), Comparative Effects of migrating solar sources on tidal signatures in the middle and upper atmosphere, *J. Geophys. Res.*, *101*, 21,213–21,222.

Hagan, M. E., and J. M. Forbes (2002), Migrating and nonmigrating diurnal tides in the middle and upper atmosphere excited by tropospheric latent heat release, *J. Geophys. Res.*, *107*(D24), 4754, doi:10.1029/2001JD001236.

Kalnay, E., et al. (1996), The NCEP/NCAR 40-Year Reanalysis Project, *Bull. Am. Meteorol. Soc.*, *77*, 437–471.

Lott, F. (1999), Alleviation of stationary biases in a GCM through a mountain drag parametrization scheme and a simple representation of mountain lift forces, *Mon. Weather Rev.*, *127*, 788–801.

Lott, F., and M. Miller (1997), A new subgrid scale orographic drag parameterization; its testing in the ECMWF model, *Q.J.e R. Meteorol. Soc.*, *123*, 101–127.

Marcus, S. L., O. de Viron, and J. O. Dickey (2004), Atmospheric contributions to Earth nutation: Geodetic constraints and limitations of the torque approach, *J. Atm. Sci.*, *61*(3), 352–365.

Munk, W. H. and G. F. McDonald (1960), *The Rotation of the Earth*, *A Geophysical Discussion*, 323 pp., Cambridge Univ. Press, New York.

Ponte, R. M., and R. D. Ray (2002), Atmospheric pressure corrections in geodesy and oceanography: A strategy for handling air tides, *Geophys. Res. Lett.*, *29*(24), 2153, doi:10.1029/2002GL016340.

Ray, R. D., and G. D. Egbert (2004), The global S1 tide, *J. Phys. Oceanogr.*, *34*(8), 1922–1935, doi:10.1175/1520-0485.

Van den Dool, H. M., S. Saha, J. Schemm, and J. Huang (1997), A temporal interpolation method to obtain hourly atmospheric surface pressure tides in reanalysis 1979–1995, *J. Geophys. Res.*, *102*, 22,013–22,024.

Wahr, J. M. (1982), The effects of the atmosphere and oceans on the Earth's wobble, 1, Theory, *Geophys. J.R. Astron. Soc.*, *70*(2), 329–372.

V. Dehant, O. de Viron, and G. Schwarzbaum, Royal Observatory of Belgium, Avenue circulaire, 3, Brussels, B-1180, Belgium. (v.dehant@oma.be; o.deviron@oma.be)

F. Lott, Ecole Normale Supérieure, Boite 99, 4 place Jussieu, F-75252 Paris, France. (flott@lmd.ens.fr)

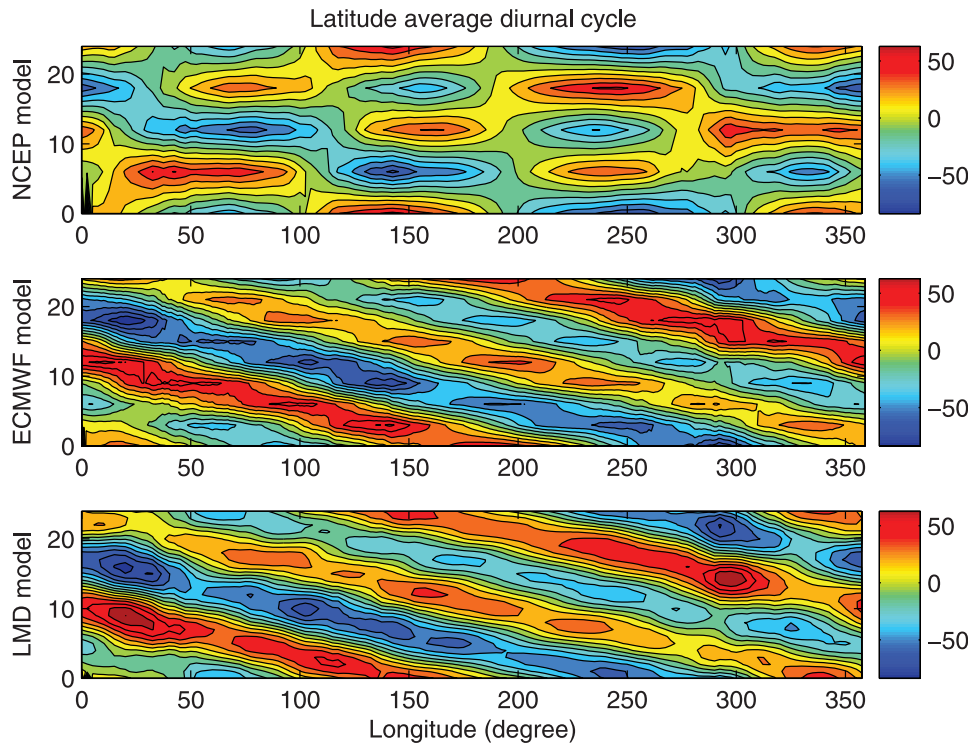

Figure 1. Latitude averaged pressure variation (in Pa) for the three models. The *y* axis is the time of the day, in hours.

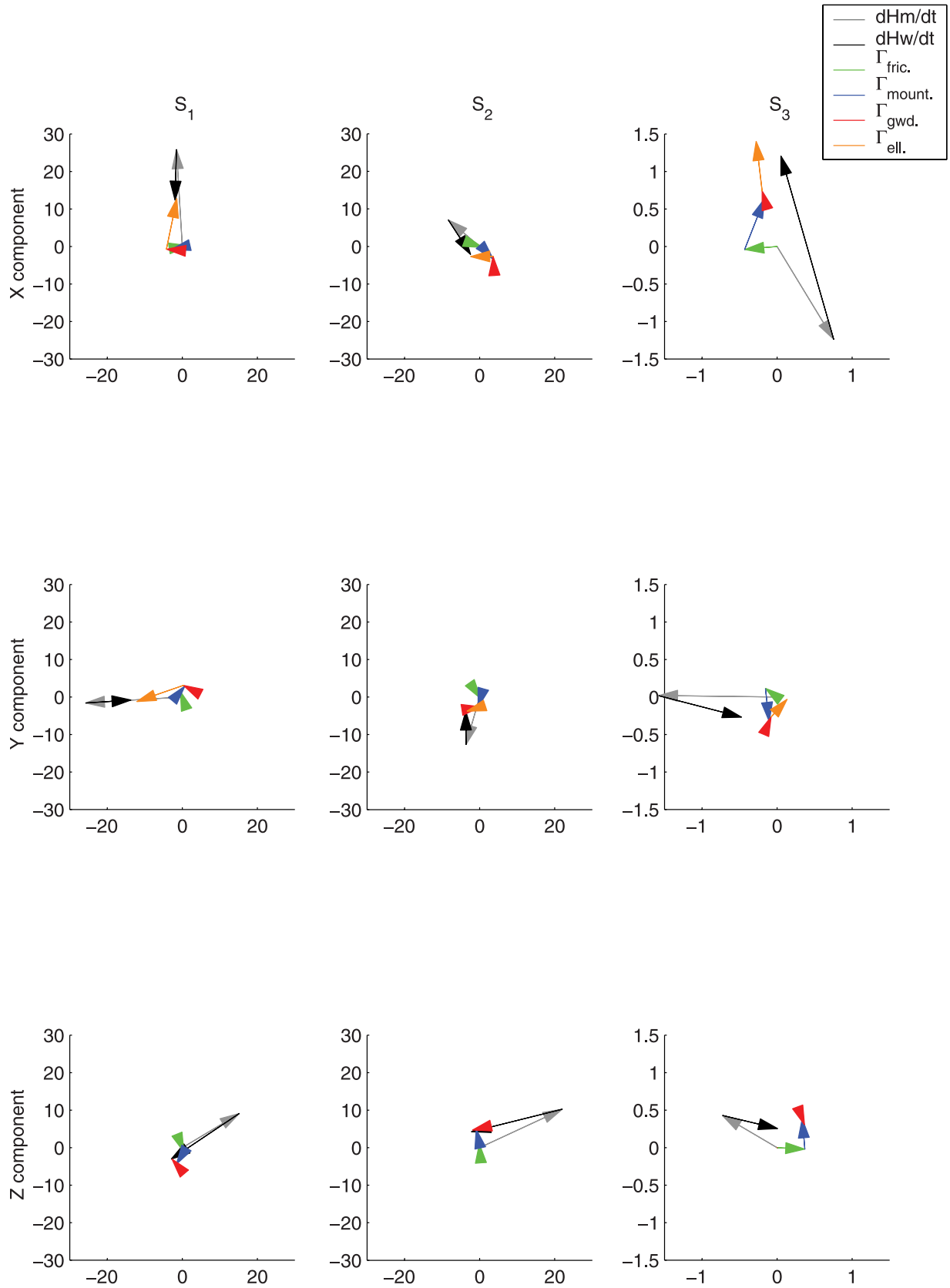

Figure 4. Phasor plot of the angular momentum budget, the phase is with respect to 0000 UT (unit hadleys, i.e., 10^{18} N m). The *X* component is the AAM budget closure in phase with the civil time, and the *Y* component is the AAM budget in quadrature.

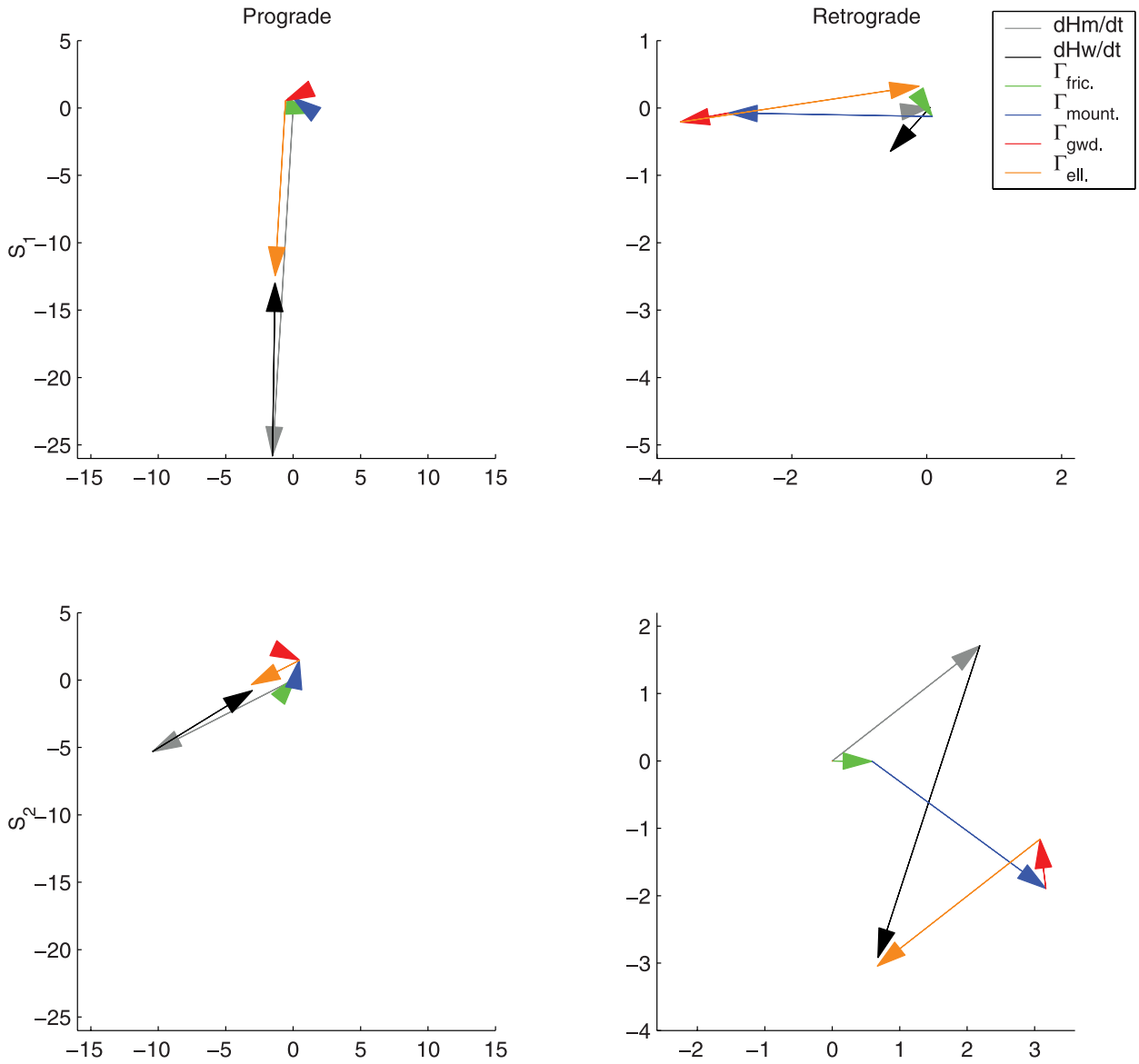

Figure 5. Phasor plot of the equatorial angular momentum budget expressed in terms of prograde and retrograde terms, the phase is with respect to 0000 UT (unit hadleys, i.e., 10^{18} N m).